

# First observation of the magnetic dipole CO<sub>2</sub> absorption band at 3.3 μm in the atmosphere of Mars by the ExoMars Trace Gas Orbiter ACS instrument

A. Trokhimovskiy<sup>1</sup>, V. Perevalov<sup>2</sup>, O. Koralev<sup>1</sup>, A. A. Fedorova<sup>1</sup>, K. S. Olsen<sup>3,4</sup>, J.-L. Bertaux<sup>1,3</sup>, A. Patrakeev<sup>1</sup>, A. Shakun<sup>1</sup>, F. Montmessin<sup>3</sup>, F. Lefèvre<sup>3</sup>, and A. Lukashevskaya<sup>2</sup>

<sup>1</sup> Space Research Institute (IKI), RAS Moscow, Russia  
e-mail: trokh@iki.rssi.ru

<sup>2</sup> V.E. Zuev Institute of Atmospheric Optics SB RAS, Tomsk, Russia

<sup>3</sup> Laboratoire Atmosphères, Milieux, Observations Spatiales (LATMOS/CNRS), Paris, France

<sup>4</sup> Department of Physics, University of Oxford, Oxford, UK

Received 9 April 2020 / Accepted 2 June 2020

## ABSTRACT

The atmosphere of Mars is dominated by CO<sub>2</sub>, making it a natural laboratory for studying CO<sub>2</sub> spectroscopy. The Atmospheric Chemistry Suite (ACS) on board the ExoMars Trace Gas Orbiter uses solar occultation geometry to search for minor atmospheric species. During the first year of ACS observations, the attention was focused on the spectral range covering the methane  $\nu_3$  absorption band, 2900–3300 cm<sup>-1</sup>, which has previously been observed on Mars. No methane was detected by ACS; instead, an improvement of the data processing has led to the identification of 30 weak absorption lines that were missing from spectroscopic databases. Periodic series of absorptions up to ~1.6% deep are observed systematically around the position of the methane  $Q$ -branch when the line of sight penetrates below 20 km (creating an optical path length of 300–400 km, with an effective pressure of a few millibar). The observed frequencies of the discovered lines match theoretically computed positions of the  $P$ -,  $Q$ -, and  $R$ -branches of the magnetic dipole and electric quadrupole 01111-00001 ( $\nu_2 + \nu_3$ ) absorption bands of the main CO<sub>2</sub> isotopologue; neither band has been measured or computed before. The relative depths of the observed spectral features support the magnetic dipole origin of the band. The contribution of the electric quadrupole absorption is several times smaller. Here we report the first observational evidence of a magnetic dipole CO<sub>2</sub> absorption.

**Key words.** planets and satellites: atmospheres – molecular data – techniques: spectroscopic

## 1. Introduction

Carbon dioxide is the main component of the Martian atmosphere, making up 96% of its composition. Since its discovery by ground-based spectroscopy (Kuiper 1952), spectroscopic bands of CO<sub>2</sub> in the near- and mid-infrared have been extensively used to understand the thermal structure, surface pressure, and seasonal cycles of the Martian atmosphere. It is known that the spectroscopic observations of planetary atmospheres may reveal previously unknown, weak, or forbidden spectral bands. In 2008, inconsistencies in CO<sub>2</sub> spectroscopy were reported simultaneously on Mars and Venus, initiating the discovery of the  $\nu_2 + \nu_3$  band of the <sup>16</sup>O<sup>12</sup>C<sup>18</sup>O (628) isotopologue. This band with a  $Q$ -branch near 2982 cm<sup>-1</sup> was detected at Mars by ground-based observations (Villanueva et al. 2008) and at Venus by Venus Express (Bertaux et al. 2008; Wilquet et al. 2008).

Since 2018, the Atmospheric Chemistry Suite (ACS), a three-channel spectrometer, has been operating in the orbit of Mars. It is part of the Russian contribution to the ESA-Roscosmos ExoMars Trace Gas Orbiter (TGO) mission to study the Martian atmosphere and climate (Korablev et al. 2018a). The mid-infrared channel (MIR) is optimised to address the primary science goal of the TGO mission: to obtain the most sensitive sensing of trace gases in the Martian atmosphere. To achieve this, ACS MIR has high resolving power and signal-to-noise

ratio (S/N), and operates in the spectral range of 2.3–4.2 μm, which contains characteristic absorptions of multiple Mars atmosphere gases, including trace-gas candidates. ACS MIR employs the primary observing mode of the TGO, the solar occultation sounding, taking advantage of the brightest source in the Solar System and of self-calibration. This enables a robust retrieval of vertical profiles. This technique was successfully implemented on the Venus Express and Mars Express orbiters (Bertaux et al. 2006; Nevejans et al. 2006; Korablev et al. 2006, 2012).

The spectral range of ACS MIR contains vibration-rotation bands of H<sub>2</sub>O, CO<sub>2</sub>, CO, and their isotopologues, the primary components of the Martian atmosphere. The instrument sensitivity and accuracy have been demonstrated by measuring the first vertical profiles of CO<sub>2</sub> and H<sub>2</sub>O isotopologues (Vandaele et al. 2019; Alday et al. 2019). The MIR channel is capable of measuring methane absorption features around 3018 cm<sup>-1</sup> with better accuracy than previous studies, provided methane is present in quantities above a stringent upper limit of 0.05 ppbv (Korablev et al. 2019). This is several times lower than the reported background value (Webster et al. 2018).

While ACS MIR has not detected methane so far, the high S/N and fine spectral resolution have revealed faint but distinct unknown absorption features in the same spectral range, observed at low altitudes on multiple orbits. These periodic well-spaced absorption lines have not been matched to any species

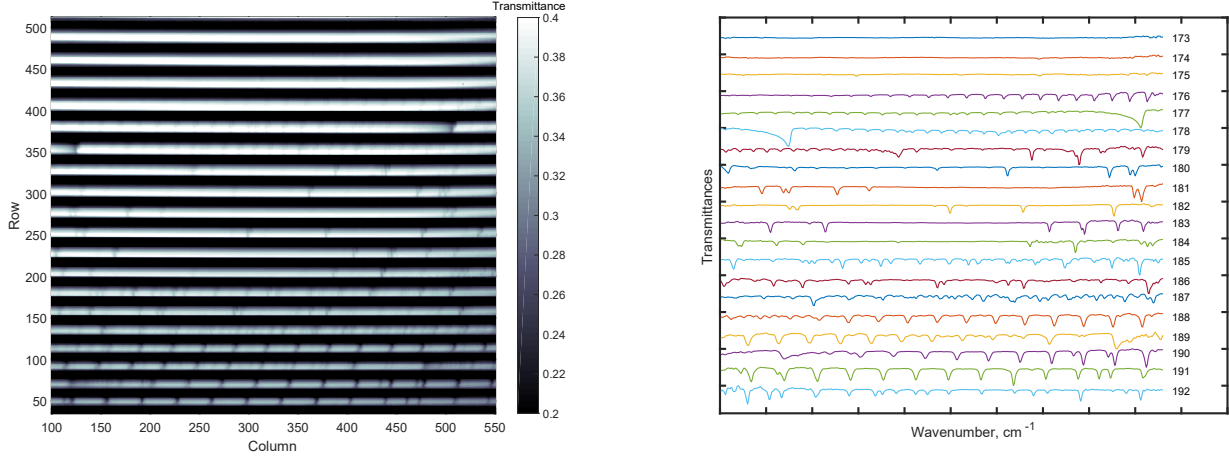


**Fig. 1.** *Left panel:* example of a single detector frame measured by ACS MIR in secondary grating position 12 after processing (orbit 6975,  $L_s = 40.3^\circ$ , tangent altitude 13 km). *Right panel:* associated series of transmission spectra, covering the wavenumber range from  $2894\text{ cm}^{-1}$  (diffraction order 173) to  $3239\text{ cm}^{-1}$  (order 192). The left and right edges of the frame in the spectral dimension, where the signal decreases, are cropped.

listed in the HITRAN [Gordon et al. \(2017\)](#) or GEISA ([Jacquinet-Husson et al. 2016](#)) databases, likely because this spectral range in Earth's atmosphere is dominated by strong methane and ozone absorptions. Theoretical considerations lead us to suspect that the observed features belong to a weak magnetic dipole 01111-000001 band of the main CO<sub>2</sub> isotopologue (<sup>12</sup>C<sup>16</sup>O<sub>2</sub>, 626) that has never been detected or measured before.

In this paper, we present a few selected ACS MIR observations that reveal the new band, and calculations for the <sup>12</sup>C<sup>16</sup>O<sub>2</sub> magnetic dipole band transitions. This discovery greatly refines spectroscopy in this spectral region of particular interest. A detailed spectroscopic study providing selection rules for the vibration-rotation spectra, calculations of line position, and measurements of line strength will be given in a dedicated paper by Perevalov et al. (in prep.). The potential effect of this additional and so far unaccounted for absorption within the methane spectral range on its detection is yet to be fully quantified. It is also compounded by the ability of ACS MIR to observe ozone absorption in the same spectral range ([Olsen et al. 2020b](#)). The ACS MIR spectrometer, observations, and occultation data processing are described in Sects. 2–4. The discovered line positions and their attribution to the magnetic dipole band of CO<sub>2</sub> are discussed in Sect. 5. In Sect. 6 we give estimated strengths of some new lines in HITRAN convention.

## 2. The instrument

On board the TGO, the Atmospheric Chemistry Suite (ACS) is a set of three spectrometers, including the novel cross-dispersion echelle ACS MIR spectrometer ([Korablev et al. 2018a](#)) that is dedicated to solar occultation measurements in the 2.2–4.4  $\mu\text{m}$  range. The resolving power, confirmed by in-flight measurements, reaches 30 000. The echelle orders are dispersed first along an  $x$ -axis and are separated along the  $y$ -axis of the focal plane by a secondary, steerable dispersion grating, making full use of the two-dimensional detector array. An example of the detector image is shown in Fig. 1. It illustrates the different diffraction orders observed across the  $y$ -axis. A stack of 200 consecutive  $640 \times 512$  pixel frames is read every 2.1 s. The combination of the instrument parameters, the aperture of F:3, the cryogenic detector, and the fast onboard frame-processing

ensures a very high S/N that reaches 10 000 for a single pixel when the unattenuated Sun is observed.

A steerable secondary grating allows choosing between different groups of diffraction orders, which changes the instantaneous spectral range. The current investigation focuses on the so-called secondary-grating position 12, which captures diffraction orders 173–192 in a single integration and covers the wavenumber range of  $2894\text{--}3239\text{ cm}^{-1}$  (see Fig. 1). This position is actively used for the methane search. The CH<sub>4</sub> *Q*-branch, centred at  $3018\text{ cm}^{-1}$ , is located in the order 180, while the *P*- and *R*-branches lie between  $2918$  and  $3140\text{ cm}^{-1}$ .

The vertical resolution for an occultation is determined by the instantaneous field of view (IFOV) of the instrument at the limb and the integration time (typically 2 s). The slit size is  $1 \times 14$  arcmin, with the long side perpendicular to the limb, resulting in an IFOV of  $\sim 6$  km for the whole slit ([Korablev et al. 2018a](#)). As the slit image covers 10–20 pixels on the detector and no binning is performed before downlink, the actual vertical resolution is some hundreds of meters.

## 3. Observations

The final TGO orbit, progressively shaped by an 18-month-long aerobraking phase in 2017 and 2018, is nearly circular, with an inclination of  $73^\circ$ , an altitude of 400 km, and a 2 h period. It was designed to maximise spatial coverage for solar occultation observations. The TGO performs occultations in an inertial pointing mode: for an ingress case, the line-of-sight (LoS) tangent altitude goes from 250 km tangent altitude until it crosses the planet. With 12 orbits per day and observations at every egress and ingress, up to 24 occultations per day can be used by TGO instruments. The latitudes covered in solar occultation range from  $88^\circ\text{N}$  to  $90^\circ\text{S}$ ; their time evolution is shown in [Korablev et al. \(2018a\)](#). In practice, ACS MIR uses only a fraction of the occultation opportunities because some orbits are dedicated to system activities or relay operations, and the occultations are shared between the ACS and NOMAD TGO instruments because their IFOVs are misaligned. For the first 1.5 yr of operation, between April 2018 and April 2020, ACS MIR observed almost 3000 occultations. Out of those, 476 observations were dedicated to the range of methane absorption using secondary-grating position 12.

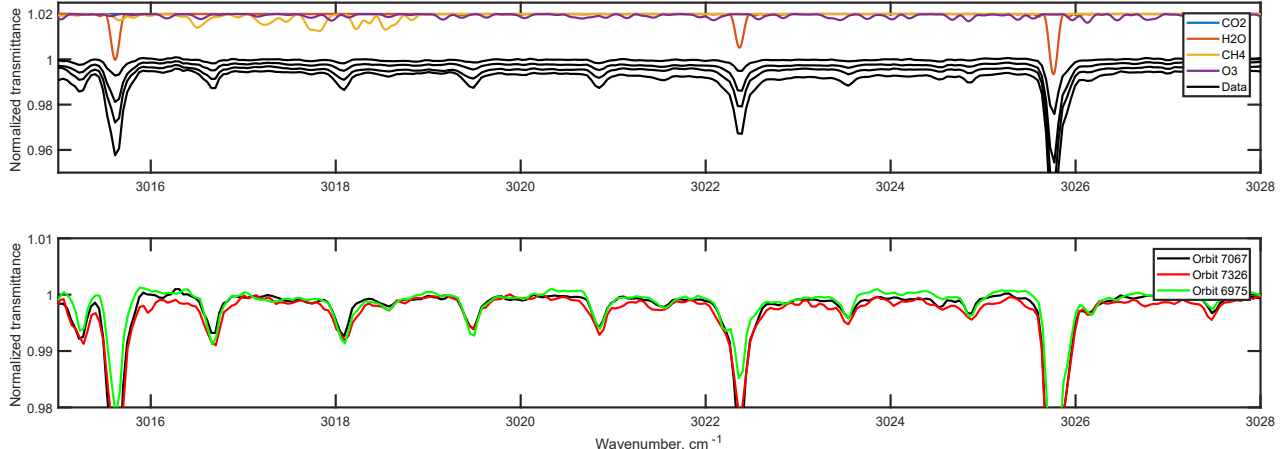


**Fig. 2.** Top panel: consecutive ACS MIR transmission spectra measured in diffraction order 180 at tangent altitudes 8–18 km (orbit 7067, black curves), against synthetic models indicating potential contributions of different atmospheric components at 10 km with MIR resolution (coloured curves): 15 ppmv of water vapour, 1 ppbv of methane, and 200 ppbv of ozone. Three  $\text{H}_2\text{O}$  lines and a series of periodic unidentified features are apparent. Bottom panel: similar spectra measured in three selected orbits (6975, 7067, and 7326) at tangent altitudes of 10 km.

While the LoS of the instrument penetrates the atmosphere, the transmission decreases owing to the gradually increasing extinction by aerosols in the Martian atmosphere. The aerosol load and its vertical extent, dependent on season and latitude (Kass et al. 2019; Stcherbinine et al. 2020), is the main limitation to detection capabilities. Toon et al. (2019) demonstrated that during an occultation, a gaseous absorption line appears with the best relative accuracy at an altitude where the LoS-integrated (or column) optical depth equals unity. The best sensitivity is therefore achieved in observations with minimum dust load, where the S/N remains high at low altitudes. In reality, if line strengths increase with decreasing temperatures, the best sensitivity can be reached at higher altitudes, where the optical depth is lower than 1 (transmittance above 0.37). In our data set, nearly 100 occultations satisfy this condition while probing below 10 km. They typically correspond to high northern and low southern latitudes. The unknown lines are observed on all such orbits. Results from a selection of the best observations (orbits 6975, 7067, and 7326), obtained in June–July 2019, at solar longitude  $L_s = 40\text{--}43^\circ$  in the southern hemisphere of Mars, are presented in this paper. The atmospheric temperature profiles necessary to compute the line strengths were retrieved from  $\text{CO}_2$  absorption lines at  $1.65\ \mu\text{m}$  observed simultaneously by the ACS near-infrared channel (NIR) (Fedorova et al. 2020).

#### 4. Data processing

We calculated the ACS MIR transmittances as a function of tangent altitude in a standard way for occultation experiments (see also Koralev et al. 2019, SSM),

$$T(z) = \frac{I(z) - I_{\text{dark}}}{I_{\text{sun}} - I_{\text{dark}}}, \quad (1)$$

where  $I$  is the signal for a given tangent altitude,  $z$ . The clear-Sun reference spectrum,  $I_{\text{sun}}$ , was obtained from the uppermost part of the occultation. A dark signal,  $I_{\text{dark}}$  (accounting for both the detector dark current and the surrounding thermal background emission), was estimated from the dark part of the occultation when the disc of Mars fully obscures the Sun. Because the thermal state of the instrument changes slightly as a result of internal and solar heating,  $I_{\text{sun}}$  and  $I_{\text{dark}}$  are time dependent. In addition, the thermal deformation causes a small (about one pixel

throughout an occultation) drift of the image on the detector. To account for the time-dependent effects, we extrapolated the trends of each pixel measured during the clear-Sun and dark signal observations through the occultation. In order to boost the accuracy of this extrapolation in the particular spectral range related to the search of  $\text{CH}_4$ , we increased the number of  $I_{\text{sun}}$  spectra, assuming that the spectral range around  $3000\ \text{cm}^{-1}$  above 100 km on Mars is mostly free of strong gaseous bands.

The level of stray light in the spectrometer does not exceed 5% near the centre of the frame, decreasing to the edges, but it unevenly affects different orders. The level of the stray light was evaluated from the signal in between the diffraction stripes. Then it was extrapolated over the frame and smoothed. We repeated the procedure for every frame before the transmittance calculation. A pixel-to-wavelength calibration was established using solar lines. It was then fine tuned to account for the drift during the occultation using the atmospheric absorption lines of  $\text{H}_2\text{O}$  or  $\text{CO}_2$  where available.

The tangent altitude was determined from the TGO SPICE kernels, and the LoS of the instrument in the body reference frame of TGO spacecraft was determined earlier in the mission by performing solar scans. For measurements used in this study, every frame was accumulated within 2.1 s, and the tangent altitude was calculated for the centre of the record.

#### 5. Identification of the unknown lines

Examples of ACS MIR spectra showing the unknown periodic features around the methane  $Q$ -branch in the diffraction order 180 are shown in Fig. 2 for some tangent altitudes and at a few favourable orbits. For these selected orbits, out of expected atmospheric contributions, only three water vapour lines appear. At the same time, periodic series of absorptions that are up to 1.6% deep show up systematically when the LoS penetrates below 20 km. The total optical path length at these tangent altitudes reaches 300–400 km, with an effective pressure of a few millibar. Initially, the existence of the unknown features in the spectra was erroneously attributed to the fixed-pattern noise that remains in the data after cleaning and processing. As the data processing improved and more orbits with little aerosol loading were measured, the absorption nature of the unidentified lines became apparent.

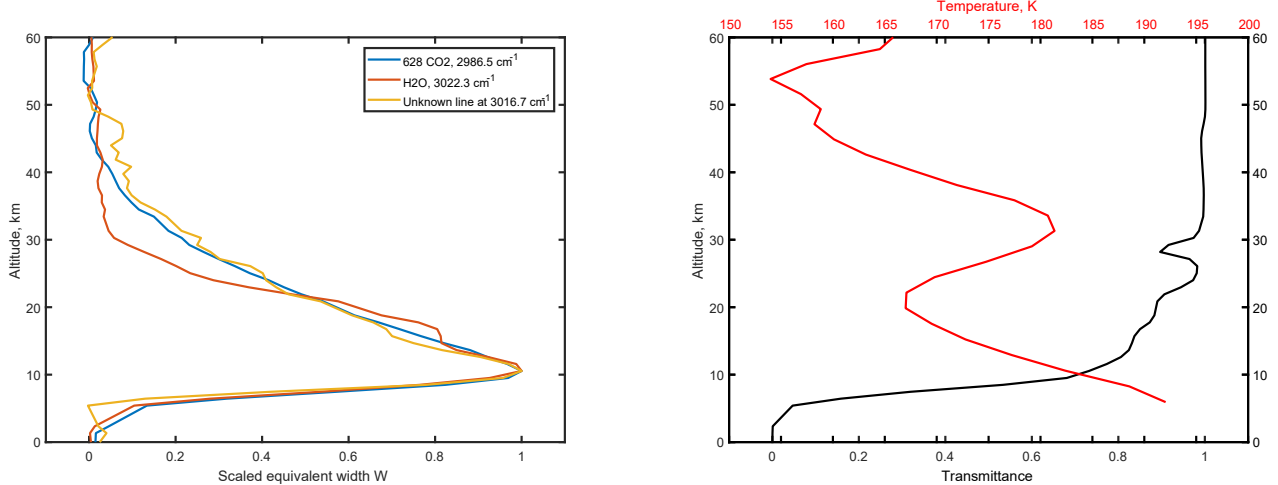


**Fig. 3.** *Left panel:* evolution of the equivalent width of one unknown line ( $3016.7 \text{ cm}^{-1}$ ) during an occultation (orange curve) against the equivalent widths of a neighbouring  $\text{H}_2\text{O}$  line ( $3022.3 \text{ cm}^{-1}$ ) from order 180 and a  $\text{CO}_2$  line ( $2986.5 \text{ cm}^{-1}$ ) from order 178. *Right panel:* corresponding temperature profile from simultaneously observed ACS NIR data. The continuum transmittance is presented in the right panel for reference. Orbit 7326 is shown.

Unlike other AOTF-echelle spectrometers used in planetary missions (Korablev et al. 2018b), ACS MIR is free from overlapping diffraction orders. The MIR detector has four video outputs so that the readout might generate a four-pixel, or a multiple of four, periodic pattern, but the unknown lines do not match this either. One of the lenses in the MIR channel appears to have been damaged during launch, resulting in a doubled image for a fraction of the slit image. This effect is minimised near the edges of the slit, where the spectra presented here were taken (Alday et al. 2019). This doubling is used to verify that the lines are real, external to the instrument and spacecraft, and are only caused by the observed scene.

The spacing between the unknown lines varies slightly. It increases for lower wavenumbers, similar to a gaseous absorption line system. It is twice greater than the spacing of the  $R$ -branch  $628 \text{ CO}_2$  isotopologue band located at smaller wavenumbers (see below), which means that they cannot result from potential cross-talk between diffraction orders, or distant lines of nearby, strong  $\text{CO}_2$  bands. Nevertheless, the periodic nature of the observed features suggests a linear or diatomic molecule. From the line-to-line distance, we estimate the value of the rotational constant,  $0.7\text{--}0.8 \text{ cm}^{-1}$ . It is close to the rotational constants of  $\text{ClO}$  and  $\text{SO}$  molecules. Both species, exotic for the Martian atmosphere, are missing in the HITRAN database in this range.

We furthermore investigated the vertical trends of the unknown lines. In Fig. 3 we compare the line depths of the new lines to those of other species present in the spectral range. The equivalent width of a neighbouring  $\text{H}_2\text{O}$  line varies with altitude following the atmospheric temperature (see Fig. 3, right panel), while the unknown line depth is strongly correlated to the  $628 \text{ CO}_2$  absorption. The candidate absorber is therefore well mixed or belongs to one of the  $\text{CO}_2$  isotopologues.

Spectroscopic computations suggest that the observed lines can be attributed to the 01111-00001 absorption band of the main 626 isotopologue. The positions of theoretically computed lines in  $P$ -,  $Q$ -, and  $R$ -branch lines exactly match the features in observed spectra.

This band is forbidden in the electric dipole absorption, but it is allowed in the electric quadrupole and the magnetic dipole absorptions. The lines due to these mechanisms are expected to be very weak (Goldman et al. 1981; Boreiko et al. 1984), and

**Table 1.** Calculated line positions of the 01111-00001 magnetic dipole absorption band of  $^{12}\text{C}^{16}\text{O}_2$  (the uncertainties of the calculated line positions are within  $0.001 \text{ cm}^{-1}$ ).

$J$	$\nu (\text{cm}^{-1})$ , $P$ -branch	$\nu (\text{cm}^{-1})$ , $Q$ -branch	$\nu (\text{cm}^{-1})$ , $R$ -branch
0	–	–	3004.789
2	3002.447	3003.996	3006.329
4	3000.866	3003.960	3007.854
6	2999.269	3003.902	3009.361
8	2997.655	3003.823	3010.853
10	2996.026	3003.723	3012.329
12	2994.380	3003.603	3013.787
14	2992.718	3003.461	3015.230
16	2991.040	3003.298	3016.656
18	2989.346	3003.114	3018.066
20	2987.637	3002.909	3019.459
22	2985.911	3002.683	3020.835
24	2984.169	3002.436	3022.195
26	2982.411	3002.168	3023.539
28	2980.637	3001.879	3024.865
30	2978.847	3001.569	3026.175
32	2977.041	3001.237	3027.469
34	2975.219	3000.885	3028.745
36	2973.382	3000.512	3030.005

they have never been observed before for  $\text{CO}_2$  in laboratory or field experiments.

We calculated the line positions for this band within the framework of the effective operator approach (Teffo et al. 1992; Tashkun et al. 1998) using effective Hamiltonian parameters published by Majcherova et al. (2005). The results are presented in Table 1. In the electric quadrupole absorption, this  $\Delta\ell_2 = 1$  band has five branches:  $O$  ( $\Delta J = -2, e \rightarrow e$ ),  $P$  ( $\Delta J = -1, e \rightarrow f$ ),  $Q$  ( $\Delta J = 0, e \rightarrow e$ ),  $R$  ( $\Delta J = 1, e \rightarrow f$ ), and  $S$  ( $\Delta J = 2, e \rightarrow e$ ). Here,  $J$  is the total angular momentum quantum number,  $\ell_2$  is the vibrational angular momentum quantum number, and  $e$  and  $f$  are the parity labels. In the magnetic dipole absorption, the band has three branches:  $P$  ( $\Delta J = -1, e \rightarrow f$ ),  $Q$  ( $\Delta J = 0, e \rightarrow e$ ), and  $R$  ( $\Delta J = 1, e \rightarrow f$ ). These selection rules

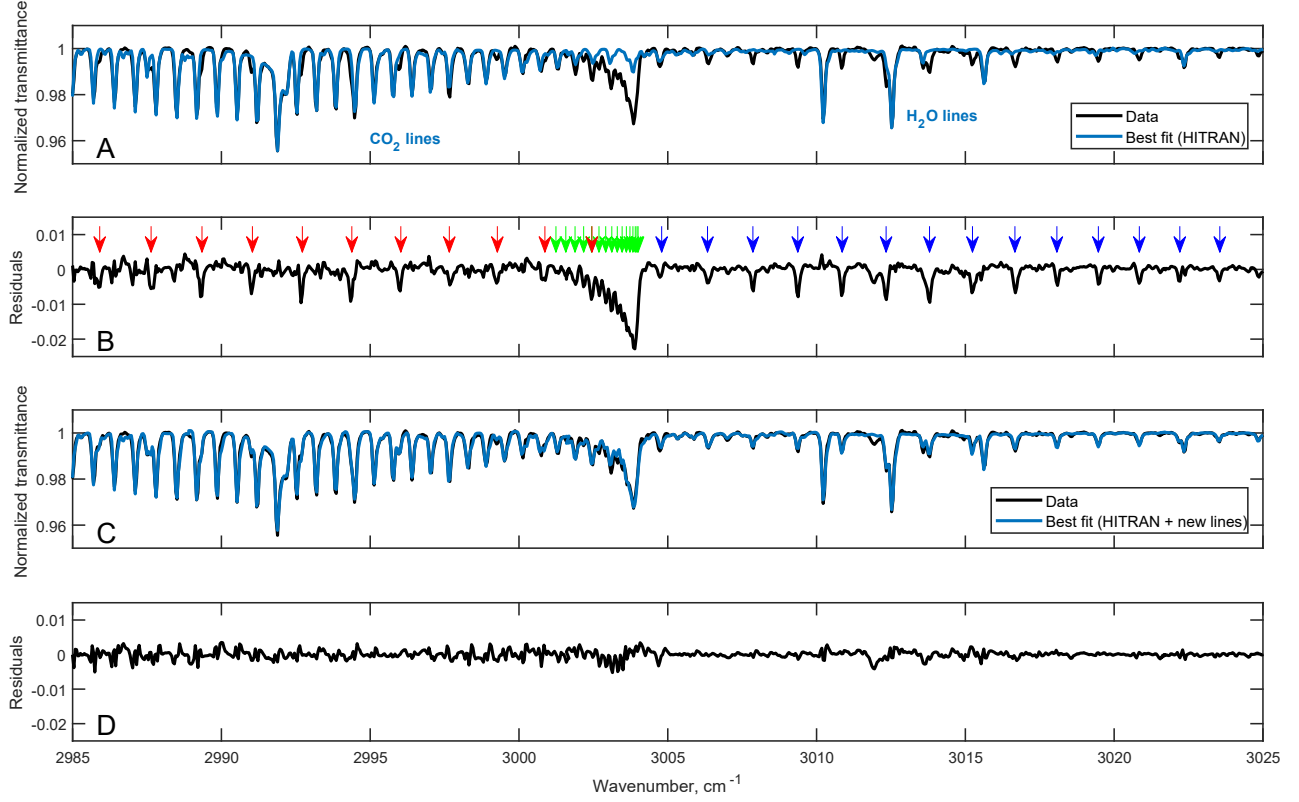


**Fig. 4.** Full extent of the discovered 626  $\text{CO}_2$  magnetic dipole band. *Panel A*: combination of ACS MIR spectra observed in diffraction orders 178–180, with a best-fit synthetic model containing apparent contributions of the  $\text{CO}_2$  and  $\text{H}_2\text{O}$  based on HITRAN 2016 database. *Panel B*: residual, revealing the structure of the 01111-00001 626 absorption band with  $P$ -,  $Q$ - and  $R$ -branches. Calculated line positions are marked with red ( $P$ ), green ( $Q$ ), and blue ( $R$ ) arrows. The example spectrum was recorded in orbit 6975 ( $L_s = 40.3^\circ$ ,  $70.9^\circ\text{N}$ ,  $21.6^\circ\text{W}$ ) and corresponds to the tangent altitude of 10.4 km. *Panel C*: best-fit synthetic model accounting for the new lines with corresponding residuals in *panel D*.

shows that the line positions for the  $P$ -,  $Q$ -, and  $R$ -branches of both absorption mechanisms do coincide. The line intensities are proportional to the transition moment squared, described as

$$W_{01111\epsilon' J+\Delta J \leftarrow 00001e} = \left| \langle 01111\epsilon' | (T_1^{(\omega)})^{eff} | 00001e \rangle \right|^2 {}^{(\omega)}H_{\Delta J}^{(\Delta K=1)}(J), \quad (2)$$

neglecting the vibration-rotation interactions. Here  $\epsilon'$  is the parity label for the upper vibrational state,  $T_1^{(2)} = Q_1^{(2)}$  is the spherical component of the electric quadrupole tensor in the case of the electric quadrupole absorption, and  $T_1^{(1)} = M_1^{(1)}$  is the spherical component of the magnetic dipole moment vector in the case of the magnetic dipole absorption. The Hönl-London factors  ${}^{(\omega)}H_{\Delta J}^{(\Delta K=1)}(J)$  are given in Table 2. Our forthcoming paper reports that (Perevalov et al., in prep.) these Hönl-London factors  ${}^{(\omega)}H_{\Delta J}^{(\Delta K=1)}(J)$  are connected with the Clebsch-Gordan coefficients  $(\omega 1J0|J+\Delta J1)$  by the equation

$${}^{(\omega)}H_{\Delta J}^{(\Delta K=1)}(J) = (2J+1)(\omega 1J0|J+\Delta J1)^2. \quad (3)$$

Both absorption mechanisms contribute to the intensities of the observed lines. We do not know the values of either the spherical component matrix elements of the electric quadrupole tensor or the magnetic dipole moment vector, to decide which absorption mechanism dominates for the observed lines. In the symmetric 626 molecule, the magnetic dipole moment is absent in the ground-vibrational state. However, it appears in the doubly degenerated vibration because it generates the vibrational

**Table 2.** Hönl-London factors for the  $\Delta\ell_2=1$  magnetic dipole and electric quadrupole  $^{12}\text{C}^{16}\text{O}_2$  absorption bands originating from the ground-vibrational state (Perevalov et al., in prep.).

	Magnetic dipole band	Electric quadrupole band
$O$ -branch	–	$\frac{J(J-2)}{2J-1}$
$P$ -branch	$\frac{J-1}{2}$	$\frac{J+1}{2}$
$Q$ -branch	$\frac{2J+1}{2}$	$\frac{3}{2} \frac{(2J+1)}{(2J-1)(2J+3)}$
$R$ -branch	$\frac{J+2}{2}$	$\frac{J}{2}$
$S$ -branch	–	$\frac{(J+1)(J+3)}{2J+3}$

angular momentum described by the quantum number  $\ell_2$ . The analysis of the Hönl-London factors (see Table 2) shows that the magnetic dipole absorption band has a relatively strong  $Q$ -branch compared to the  $P$ - and  $R$ -branches. At the same time, for the electric quadrupole band, the intensities of  $O$ - and  $S$ -branches are comparable to the  $P$ - and  $R$ -branches, while the  $Q$ -branch is significantly weaker.

In a search for more spectral signatures of the new band, we have studied several diffraction orders, adjacent to order 180, and compared the experimental data to a synthetic model including contributions of all known components of the Martian atmosphere, as described in a paper by Olsen et al. (2020a). Panel A in Fig. 4 shows spectra covering orders 178–180, and a computed fit with the JPL Gas Fitting Software suite (GGG or

GFIT; Irion et al. 2002; Wunch et al. 2011) using HITRAN 2016 (Gordon et al. 2017); temperature and pressure vertical profiles are taken from the ACS NIR channel (Fedorova et al. 2020). The difference between the experimental data and the best-fit model (Fig. 4B) shows a prominent  $Q$ -branch of the new band at 3002–3004 cm $^{-1}$ , and multiple  $P$  lines at smaller wavenumbers. The  $O$ - and  $S$ -branches, which should be in the regions 2945–2998 and 3006–3058 cm $^{-1}$ , respectively, are not detected. We therefore conclude that the observed lines originate from a magnetic dipole. The contribution of the electric quadrupole transitions should be several times smaller at least.

## 6. Line strengths

Unlike the positions, line strengths cannot be computed a priori using the effective operator approach. We may estimate them from the intensities of nearby known lines. The equivalent width  $W$  of a line in a transmission spectrum, independent of the instrumental resolution, is

$$W = \int \frac{T_c - T(\nu)}{T_c} d\nu, \quad (4)$$

where the integral is over a wavenumber interval encompassing the line,  $T_c$  is the continuum transmission, and  $T(\nu)$  is the transmission in the line. The strength of a non-saturated absorption feature is defined as  $S_Q = W/N$ , where  $N$  is the number of molecules at the LoS. For a given temperature, the line strength of an unknown line can be estimated as

$$S_Q = S_Q(\text{known line}) * W/W(\text{known line}). \quad (5)$$

In order to minimise the influence of the instrument line shape function and other factors on the retrieved line strengths, we selected as the reference the closest CO<sub>2</sub> band, which belongs to the 628 isotopologue with the  $Q$ -branch at 2982 cm $^{-1}$ . The HITRAN convention (Rothman et al. 2005) incorporates standard terrestrial fractionation factors of an isotopologue in their line strengths (De Biévre et al. 1984). In order to use the 628 line strengths to determine the line strengths of the 626 magnetic dipole lines in our observations, we accounted for the 628/626 ratio on Mars. The terrestrial 628/626 ratio is  $4.01 \times 10^{-3}$ , this accounts for two O atoms in the CO<sub>2</sub> molecule. The CO<sub>2</sub> isotopes on Mars were measured by Krasnopolsky (2007) and found to be very close to the telluric:  $^{18}\text{O}/^{16}\text{O} = 1.02 \pm 0.02$  times the terrestrial standard. Furthermore, a small enrichment of the  $^{18}\text{O}/^{16}\text{O}$  ratio in the Martian water vapour has recently been found from ACS MIR measurements (Alday et al. 2019). We, therefore, assume  $^{16}\text{O}^{12}\text{C}^{18}\text{O}/^{16}\text{O}^{12}\text{C}^{16}\text{O}$  ratio for our measurements to be 1.02 times the terrestrial one and use this factor while comparing the equivalent widths.

To estimate the line strength of the 3016.656 cm $^{-1}$   $R$ -branch line ( $J=16$ ), we selected a reference 628 CO<sub>2</sub> line at 2986.42 cm $^{-1}$  (R5 line of the 01111-00001 band). This line is close to the investigated line at the detector, and it is free from other absorptions. In addition, the vertical intensity profiles of the two selected lines (see Sect. 5) are comparable, suggesting that their temperature dependencies are also similar and would not introduce additional uncertainties to the estimation. We considered spectra recorded at an altitude of 15 km, where the retrieved ACS NIR temperature (Fedorova et al. 2020) is 172 K. The HITRAN 2016 (Gordon et al. 2017) line list indicates a line strength  $S_Q(R5$  of the 628 magnetic dipole band)= $1.77 \times 10^{-27}$  cm molecule $^{-1}$  for this temperature. The

**Table 3.** Measured positions and their estimated line intensities of the 01111-00001  $^{12}\text{C}^{16}\text{O}_2$  magnetic dipole band.

Line	Theoretical wavenumber (cm $^{-1}$ )	Retrieved wavenumber (cm $^{-1}$ )	$S_Q \times 10^{28}$ cm molecule $^{-1}$ at 172 K	$S_Q \times 10^{28}$ cm molecule $^{-1}$ at 296 K
R16	3016.656	3016.66	6.9	5.4
R18	3018.066	3018.07	6.4	5.5
R20	3019.459	3019.46	5.3	5.1
R22	3020.835	3020.84	4.3	4.6

**Notes.** The line intensities are given in the HITRAN convention (the isotopic abundance is 0.9842).

equivalent widths of the known CO<sub>2</sub> line and of the new line are 0.0644 and 0.0246, respectively. By this, the derived value of  $S_Q$  is

$$S_Q = (1.77 \times 10^{-27} \times 0.0246/0.0644) \times 1.02 = 6.9 \times 10^{-28} \text{ cm molecule}^{-1}. \quad (6)$$

We applied a similar procedure to some other nearby well-resolved lines of the new band; the results are listed in Table 3. The line strengths were also recomputed for the reference HITRAN temperature of 296 K using the well-known equation (e.g. Rothman et al. 2010). This table also contains wavenumbers of the new lines retrieved from ACS MIR experimental data. The uncertainties are of order 0.01 cm $^{-1}$ , greater than the uncertainties of theoretical values, but the consistency is undeniable.

Using the standard equation for the line intensity of the magnetic dipole absorption (e.g. Boreiko et al. 1984) and Eq. (2) for the magnetic dipole transition moment squared, we fitted the vibrational transition moment squared to line intensities of the four observed lines. The fitted value of this parameter  $\langle |01111\varepsilon'| (T_1^{(\omega)})^{\text{eff}} |00001e\rangle|^2 = 2.367(26) \times 10^{-11} D^2$  was then used to calculate the intensities of other lines up to  $J=60$  for two temperatures of 172 and 296 K. The sum of all line intensities gives the integrated band intensity for these two temperatures:  $S(172\text{ K}) = 2.89 \times 10^{-26}$  cm molecule $^{-1}$  and  $S(296\text{ K}) = 2.69 \times 10^{-26}$  cm molecule $^{-1}$ . Figure 4 shows a synthetic best-fit model spectrum constructed using the estimated intensities of all the new lines, and the greatly reduced residual of the fit (panels C and D). A detailed analysis and the list of the line intensities, corroborated by laboratory measurements, will be presented in Perevalov et al. (in prep.).

## 7. Conclusions

The observed 01111-00001 magnetic dipole band of  $^{16}\text{O}^{12}\text{C}^{16}\text{O}$  is to our knowledge the first experimental manifestation of the importance of the nuclear motion contribution to the molecular magnetic dipole moment. This  $v_2 + v_3$  band, the same as identified in 2008 at Venus (Bertaux et al. 2008; Villanueva et al. 2008) for the 628 CO<sub>2</sub> isotopologue, is forbidden in the symmetric carbon dioxide species. For the 628 magnetic dipole band, it exists because  $^{18}\text{O}$  breaks the symmetry of the molecule. For the main isotopologue, it exists because of the magnetic dipole.

We observed this new band in the very clean atmosphere of Mars. The trace gases (methane, ethylene, water vapour, and ozone) of the Earth atmosphere have strong bands in the studied region. This leaves little opportunity to detect this band in

the atmospheres of other planets using ground-based telescopes. This band can be sought in the SOIR/Venus Express occultation data set, although the range appears difficult because of overlapping diffraction orders (Vandaele et al. 2013). Our initial search gave no results. In the low atmosphere of Venus, hot carbon dioxide bands (Rothman et al. 2010) are superimposed on the magnetic dipole absorption.

This first observation of the magnetic dipole carbon dioxide band in the Martian atmosphere, though very weak, has a fundamental interest from the molecular spectroscopy point of view and is essential in the carbon dioxide-rich cold atmospheres, including Earth-like exoplanets. It also shows that the HITRAN and GEISA databases have to be extended by including the line parameters for the magnetic dipole bands of carbon dioxide.

The spectral position of the new band overlaps the strongest *Q*- and *R*-branch transitions of methane absorption used in the survey on Mars. Together with the effect of ozone in the same spectral range (Olsen et al. 2020b), this discovery secures a new framework, increasing the sensitivity and reliability of all ongoing and future studies aimed at detecting methane or setting stringent upper limits. With these measurements, the MIR channel of ACS sets a new standard for the observations of planetary atmospheres, fulfilling the main goal of the TGO mission by characterising minor species (assuming the CO<sub>2</sub> isotopologue can be considered as a minor species) in unprecedented detail.

**Acknowledgements.** ExoMars is a space mission of ESA and Roscosmos. The ACS experiment is led by IKI, the Space Research Institute in Moscow, assisted by LATMOS in France. The project acknowledges funding by Roscosmos and CNES. The science operations of ACS are funded by Roscosmos and ESA. We are grateful to a large number of people responsible for designing, building, testing, launching, communicating to and operating the spacecraft and science instruments of TGO. A.T., O.K. and A.F. acknowledge RSF funding under grant number 20-42-09035 for work described in Sects. 5 and 6. LATMOS affiliates acknowledge funding from CNES. K.S.O. acknowledges funding from the Natural Sciences and Engineering Research Council of Canada (NSERC) (PDF – 516895 – 2018) and the UK Space Agency (ST/T002069/1).

## References

- Alday, J., Wilson, C. F., Irwin, P. G. J., et al. 2019, *A&A*, **630**, A91  
 Bertaux, J.-L., Koralev, O., Perrier, S., et al. 2006, *J. Geophys. Res.*, **111**, E10S90  
 Bertaux, J.-L., Vandaele, A. C., Wilquet, V., et al. 2008, *Icarus*, **195**, 28
- Boreiko, R. T., Smithson, T. L., Clark, T. A., & Wieser, H. 1984, *J. Quant. Spectr. Rad. Transf.*, **32**, 109  
 De Biévre, P., Gallet, M., Holden, N. E., & Barnes, I. L. 1984, *J. Phys. Chem. Ref. Data*, **13**, 809  
 Fedorova, A. A., Montmessin, F., Koralev, O., et al. 2020, *Science*, **367**, 297  
 Goldman, A., Reid, J., & Rothman, L. S. 1981, *Geophys. Res. Lett.*, **8**, 77  
 Gordon, I. E., Rothman, L. S., Hill, C., et al. 2017, *J. Quant. Spectr. Rad. Transf.*, **203**, 3  
 Irion, F. W., Gunson, M. R., Toon, G. C., et al. 2002, *Appl. Opt.*, **41**, 6968  
 Jacquinot-Husson, N., Armante, R., Scott, N. A., et al. 2016, *J. Mol. Spectr.*, **327**, 31  
 Kass, D. M., Schofield, J. T., Kleinböhl, A., et al. 2019, *Geophys. Res. Lett.*, **46**  
 Koralev, O., Bertaux, J.-L., Fedorova, A., et al. 2006, *J. Geophys. Res.*, **111**, E09S03  
 Koralev, O. I., Fedorova, A. F., Bertaux, J.-L., et al. 2012, *Planet. Space Sci.*, **65**, 38  
 Koralev, O., Montmessin, F., Trokhimovskiy, A., et al. 2018a, *Space Sci. Rev.*, **214**, 7  
 Koralev, O. I., Belyaev, D. A., Dobrolenskiy, Y. S., Trokhimovskiy, A. Y., & Kalinnikov, Y. K. 2018b, *Appl. Opt.*, **57**, C103  
 Koralev, O., Vandaele, A. C., Montmessin, F., et al. 2019, *Nature*, **568**, 517  
 Krasnopol'sky, V. A. 2007, *Icarus*, **190**, 93  
 Kuiper, G. P. 1952, *The Atmospheres of the Earth and Planets* (Chicago, US: University of Chicago Press)  
 Majcherova, Z., Macko, P., Romanini, D., et al. 2005, *J. Mol. Spectr.*, **230**, 1  
 Nevejans, D., Neefs, E., van Ransbeeck, E., et al. 2006, *Appl. Opt.*, **45**, 5191  
 Olsen, K. S., Lefèvre, F., Montmessin, F., et al. 2020a, *Nat. Geosci.*, submitted  
 Olsen, K. S., Lefèvre, F., Montmessin, F., et al. 2020b, *A&A*, **639**, A141  
 Rothman, L. S., Jacquemart, D., Barbe, A., et al. 2005, *J. Quant. Spectr. Rad. Transf.*, **96**, 139  
 Rothman, L. S., Gordon, I. E., Barber, R. J., et al. 2010, *J. Quant. Spectr. Rad. Transf.*, **111**, 2139  
 Stcherbinine, A., Vincendon, M., Montmessin, F., et al. 2020, *J. Geophys. Res.*, **125**, e06300  
 Tashkun, S. A., Perevalov, V. I., Teffo, J. L., Rothman, L. S., & Tyuterev, V. G. 1998, *J. Quant. Spectr. Rad. Transf.*, **60**, 785  
 Teffo, J. L., Sulakshina, O. N., & Perevalov, V. I. 1992, *J. Mol. Spectr.*, **156**, 48  
 Toon, G. C., Liebe, C. C., Nemati, B., et al. 2019, *Earth Space Sci.*, **6**, 836  
 Vandaele, A. C., Mahieux, A., Robert, S., et al. 2013, *Opt. Exp.*, **21**, 21148  
 Vandaele, A. C., Koralev, O., Daerden, F., et al. 2019, *Nature*, **568**, 521  
 Villanueva, G. L., Mumma, M. J., Novak, R. E., & Hewagama, T. 2008, *Icarus*, **195**, 34  
 Webster, C. R., Mahaffy, P. R., Atreya, S. K., et al. 2018, *Science*, **360**, 1093  
 Wilquet, V., Mahieux, A., Vandaele, A. C., et al. 2008, *J. Quant. Spectr. Rad. Transf.*, **109**, 895  
 Wunch, D., Toon, G. C., Blavier, J. L., et al. 2011, *Phil. Trans. R. Soc. A*, **369**, 2087